Supporting Information

Atomic Strain and Catalytic Properties of Formate Oxidation and Dehydrogenation in AgPd Nanoalloys

Tao Jin, [a, b] *Longfei Guo,* [a, b] *Quan Tang,* [a, b] *Junpeng Wang,* [a, b] *Bowei Pan,* [a, b] *Zhen Li* [a, b] *Chongyang Wang,* [a, b] *Shuang Shan,* [a, b] *and Fuyi Chen*[*, a, b]

[a] State Key Laboratory of Solidification Processing, Northwestern Polytechnical University, Xi'an 710072, China

[b] School of Materials Science and Engineering, Northwestern Polytechnical University, Xi'an, 710072, China

[*]Corresponding author: E-mail: fuyichen@nwpu.edu.cn

Details of thermodynamic calculations.

We used the method of Nørskov through the Gibbs free energy expression to investigate the effects of the electric potential on the activity and mechanism of the FOR:

$$\Delta G = \Delta H - T\Delta S = \Delta E + \Delta ZPE - T\Delta S + \Delta G_U + \Delta G_{pH} + \Delta G_{field}$$

where ΔE is the DFT total energy, T is the temperature (298.15 K) and ΔZPE and ΔS are the change in zero-point energy and entropy of the adsorbates, respectively. ΔG_U is the electrode potential (ΔG_U =eU, where U is the electrode potential with respect to the standard hydrogen electrode and e is the transferred charge). ΔG_{pH} is the pH value of the electrolyte ($\Delta G_{pH} = -k_B T \ln 10 \times pH$, where k_B is the Boltzmann constant). We used pH = 14 for an alkaline medium because of our experimental environment for FOR. ΔG_{field} is the free energy correction caused by the electrochemical double layer and is normally ignored because of its small value similar to previous studies[1–3]. The Gibbs free energy of liquid water is $\Delta G_{H20(l)} = \Delta G_{H20(g)} + RT \ln(p/p_0)$, where $\Delta G_{H20(g)}$ is calculated through DFT calculations, R is the ideal gas constant, p = 0.035 bar (saturated vapor pressure), p_0 = 1 bar, T = 298.15 K. The free energy of OH^- was obtained from the expression: $G_{OH^-} = G_{H2O(l)} - G_{H^+}$, where, $G_{H^+} = 1/2G_{H2} - k_B T \ln 10 \times pH$.

The segregation energy of Ag@Pd nanoalloy was calculated as follows:

$$E_{seg} = E_{segregated\ alloy} - E_{alloy}$$

where the $E_{segregated\ alloy}$ and E_{alloy} is the total energy of segregated alloy and unsegregated alloy with or without adsorbate.

Details of embedded atom method (EAM)[4] interatomic potential and Gupta potential.

The following is the detailed of embedded atom method (EAM) interatomic potential:

The total energy of the system is divided into two parts, one is the embedding energy of the atoms under study, and the other is the repulsion energy among all the remaining atoms forming a solid. For a system with N electrons, the total energy of the system can be expressed as:

$$E = \sum_{i=1}^{N} G_i(\rho_{h,i}) + \frac{1}{2}\sum_{i=1}^{N}\sum_{j \neq i} \phi_{ij}(R_{ij})$$

where the first term is the embedding energy, and the second term is the two-body potential.

The electron density is approximated by the superposition of atomic densities:

$$\rho_{h,i} = \sum_{j \neq i} \rho_j^a(R_{ij})$$

where $\rho_j^a(R)$ is the electron density contributed by atom j.

The atomic densities are given by:

$$\rho^a(R) = n_s\rho_s(R) + n_d\rho_d(R)$$

where n_s, and n_d are the number of outer s and d electrons and ρ_s, and ρ_d are the densities associated with the s and d wave functions.

The pair-interaction term, suggest writing the pair interaction between atoms of types A and B in terms of effective charges as:

$$\phi_{AB}(R) = Z_A(R)Z_B(R)/R$$

In EAM methods, $Z(R)$ is assumed to be a simple parametrized form:

$$Z(R) = Z_0(1 + \beta R^v)e^{-\alpha R}$$

The EAM potential parameters Z_0, α, β, v and $n_s$used in this study can be found in Reference 4.

The Gupta potential is derived from the second-moment approximation to the tight-binding (SMATB) model[5]. Within the SMATB model, the contribution to the total potential energy of atom is made up of a many-body (nonlinear) bonding term and a repulsive Born-Mayer pair term[6]. Its analytical form is defined as follows:

$$V(r_{\{ij\}}) = \sum_{i}^{N}\left(\sum_{i\neq j}^{N} Ae^{-p\bar{r}_{ij}} - \sqrt{\sum_{i\neq j}^{N}\xi^2 e^{-2q\bar{r}_{ij}}}\right)$$

where N is the number of atoms, $\bar{r}_{ij} = r_{ij}/r_0 - 1$, and r_{ij} is the distance between the atoms at sites i and j. The Gupta potential parameters A, ξ, p, q used in this study can be found in Reference 6.

Details of Atomic Strain calculations

Detail calculation steps of atomic strain are as follows:

1. The particle displacement vector U_i is calculated from the atomic coordinates of the particle in the initial and final configurations. The initial configuration is the input structure of MD simulations, and the terminated configuration is the structure after MD simulations.

2. The atomic deformation gradient tensor F is calculated for each particle.

$$F(X,t) = F_{jk} e_j \otimes I_k$$

where e_j and I_k are the unit vectors.

3. The atomic Green-Lagrangian strain tensor is calculated for each particle.

$$E = 1/2\left(F^T F - 1\right)$$

4. Calculation of atomic strain.

$$atomic\ strain = \left(E_{xx} + E_{yy} + E_{zz}\right)/3$$

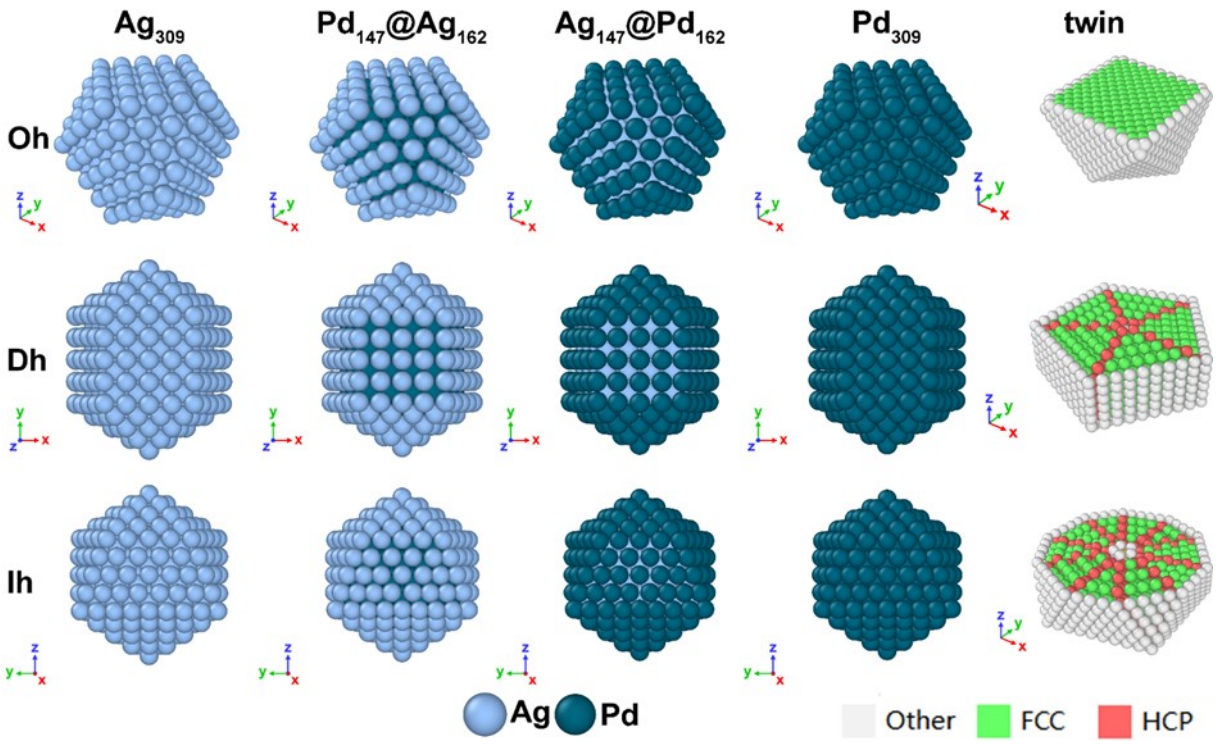

Fig. S1 The atomic structures of Ag_{309}, $Pd_{147}@Ag_{162}$, $Ag_{147}@Pd_{162}$, and Pd_{309} nanoclusters in cuboctahedron, decahedron, and icosahedron shapes donated as Oh, Dh, and Ih, respectively. A schematic diagram of the internal twinning situation is included.

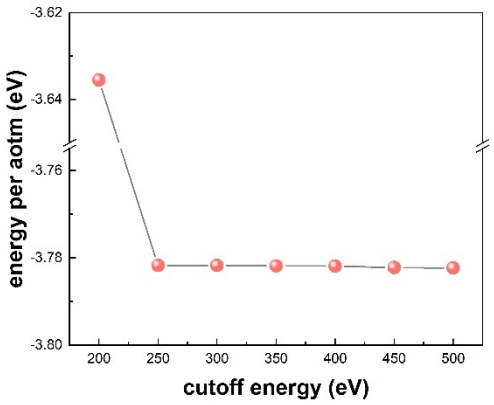

Fig. S2 The convergence test of cutoff for AgPd nanoalloys.

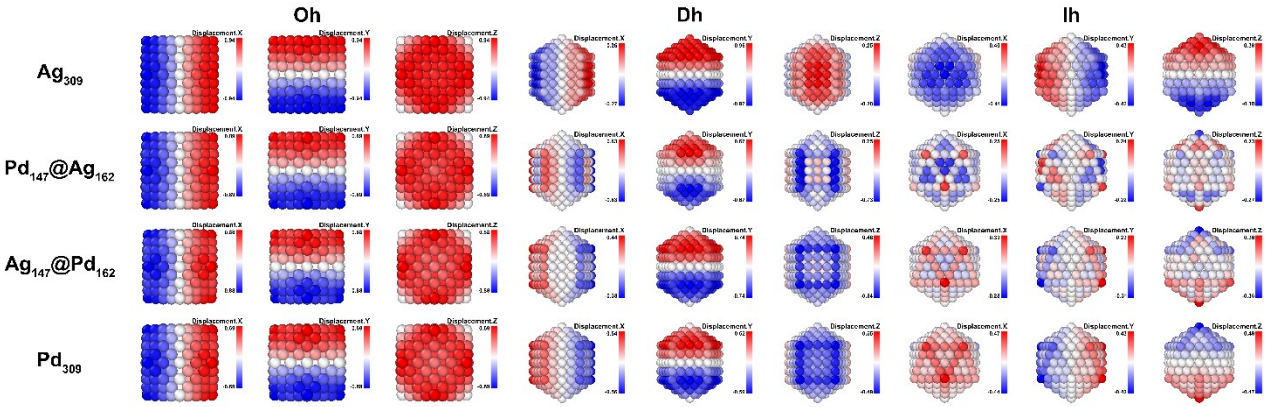

Fig. S3 The displacements of Ag_{309}, $Pd_{147}@Ag_{162}$, $Ag_{147}@Pd_{162}$, and Pd_{309} nanoalloys in cuboctahedron (Oh), decahedron (Dh), and icosahedron (Ih) shape along the x, y, and z direction after MD simulations from the initial bulk and final nanoalloy configurations.

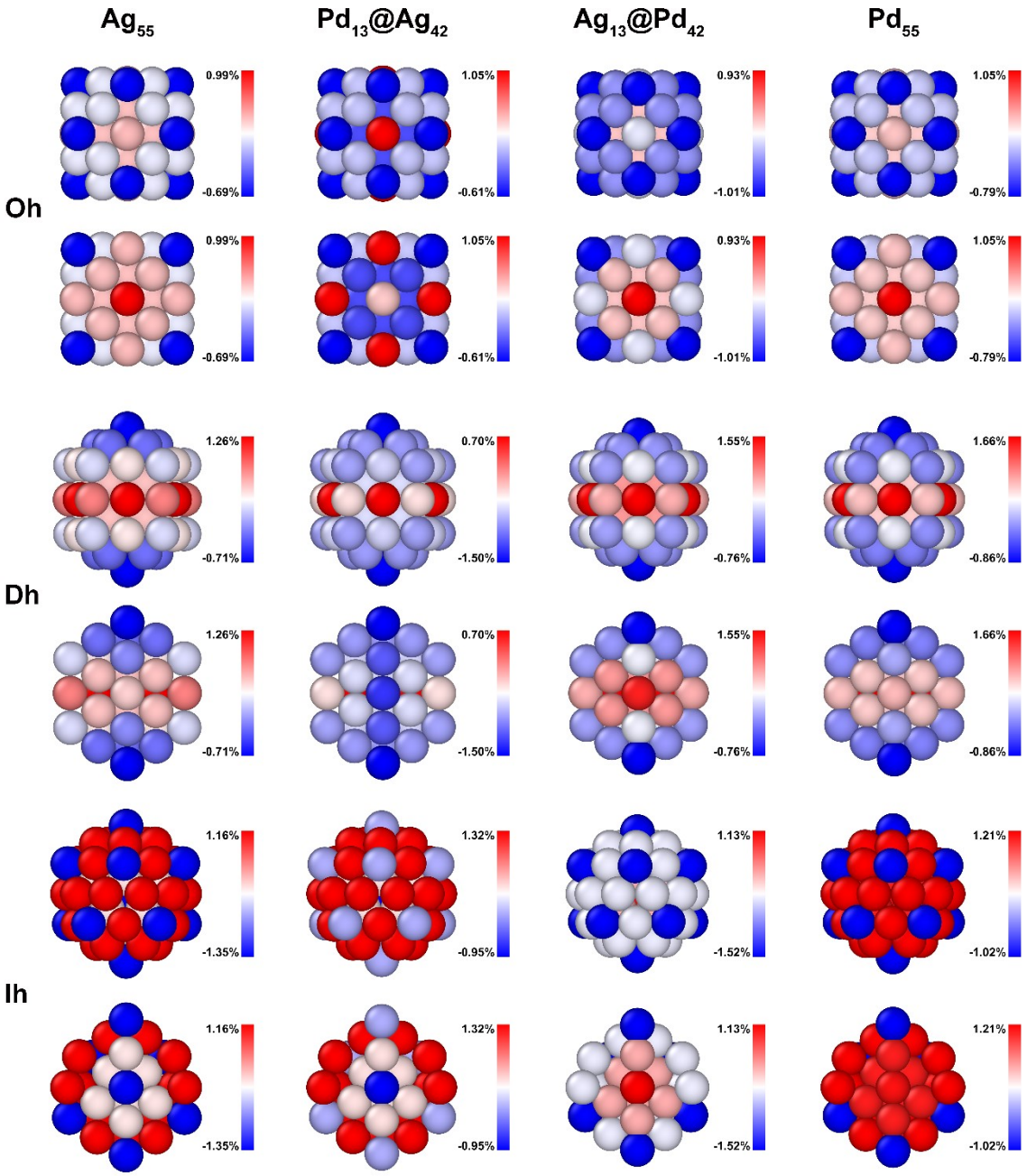

Fig. S4 The surface and cross section atomic strain fields of Ag_{55}, $Pd_{13}@Ag_{42}$, $Ag_{13}@Pd_{42}$, and Pd_{55} nanoclusters in cuboctahedron, decahedron, and icosahedron shapes, donated as Oh, Dh, and Ih, respectively. The intensity and nature of strain are represented by the color mapping: blue indicates negative values corresponding to compressive strain, while red represents positive values corresponding to tensile strain. Zero strain is represented by white. The surface strain is calculated based on the equilibrium bond length in bulk Ag and Pd.

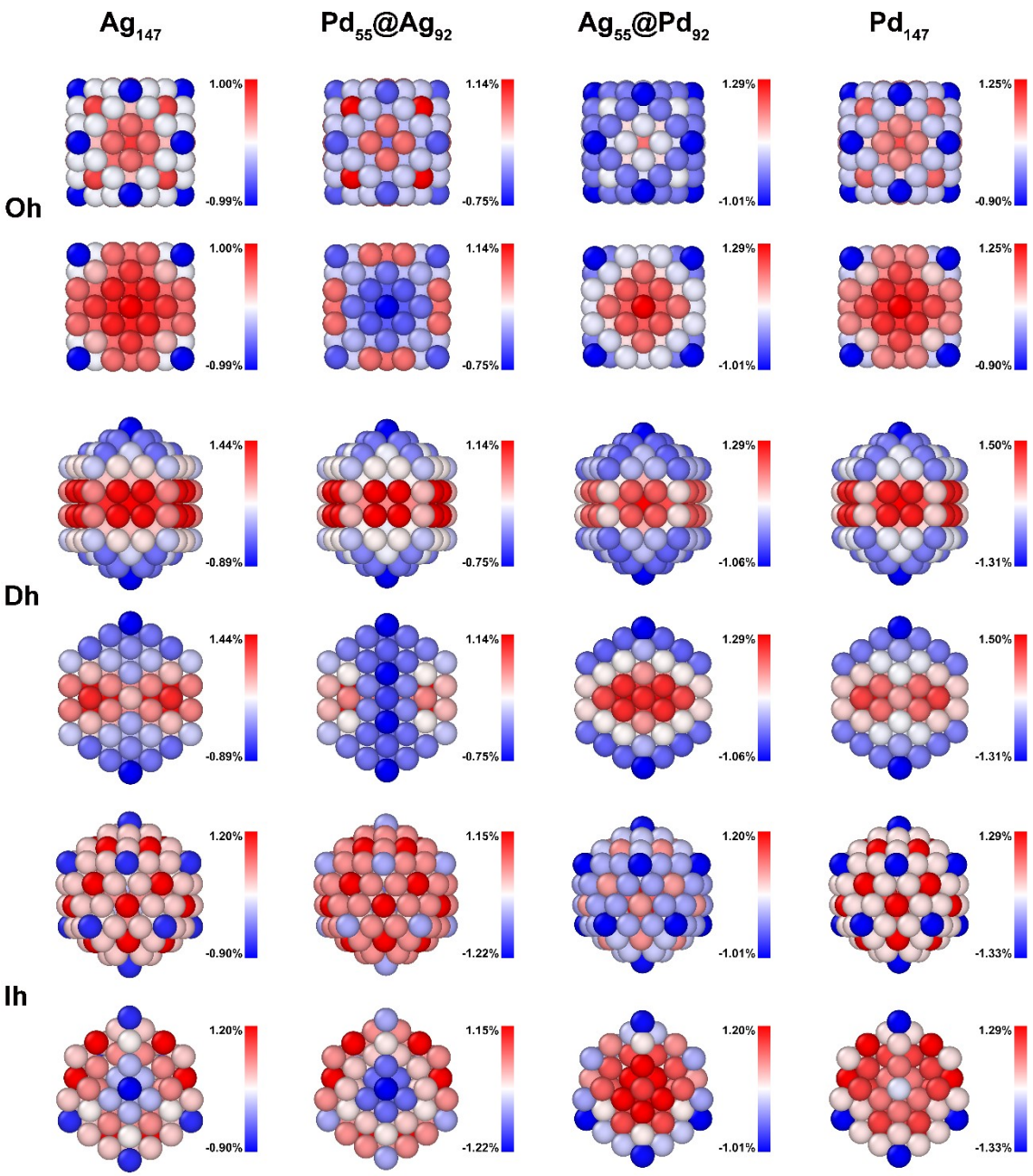

Fig. S5 The surface and cross section atomic strain fields of Ag_{147}, $Pd_{55}@Ag_{92}$, $Ag_{55}@Pd_{92}$, and Pd_{147} nanoclusters in cuboctahedron, decahedron, and icosahedron shapes, donated as Oh, Dh, and Ih, respectively. The intensity and nature of strain are represented by the color mapping: blue indicates negative values corresponding to compressive strain, while red represents positive values corresponding to tensile strain. Zero strain is represented by white. The surface strain is calculated based on the equilibrium bond length in bulk Ag and Pd.

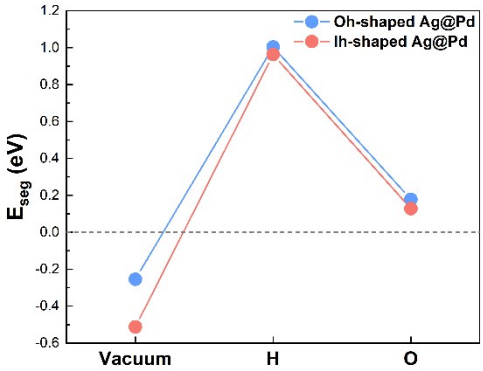

Fig. S6 The segregation energy of Oh- and Ih-shaped Ag@Pd nanoalloys under vacuum, and under the adsorption of H, and O. Ag@Pd core-shell alloys exhibit a preference for Ag surface segregation in vacuum conditions, however, it is important to note that the thermodynamic feasibility of Ag surface segregation diminishes once H intermediates are formed during formate dehydrogenation and oxidation reactions.

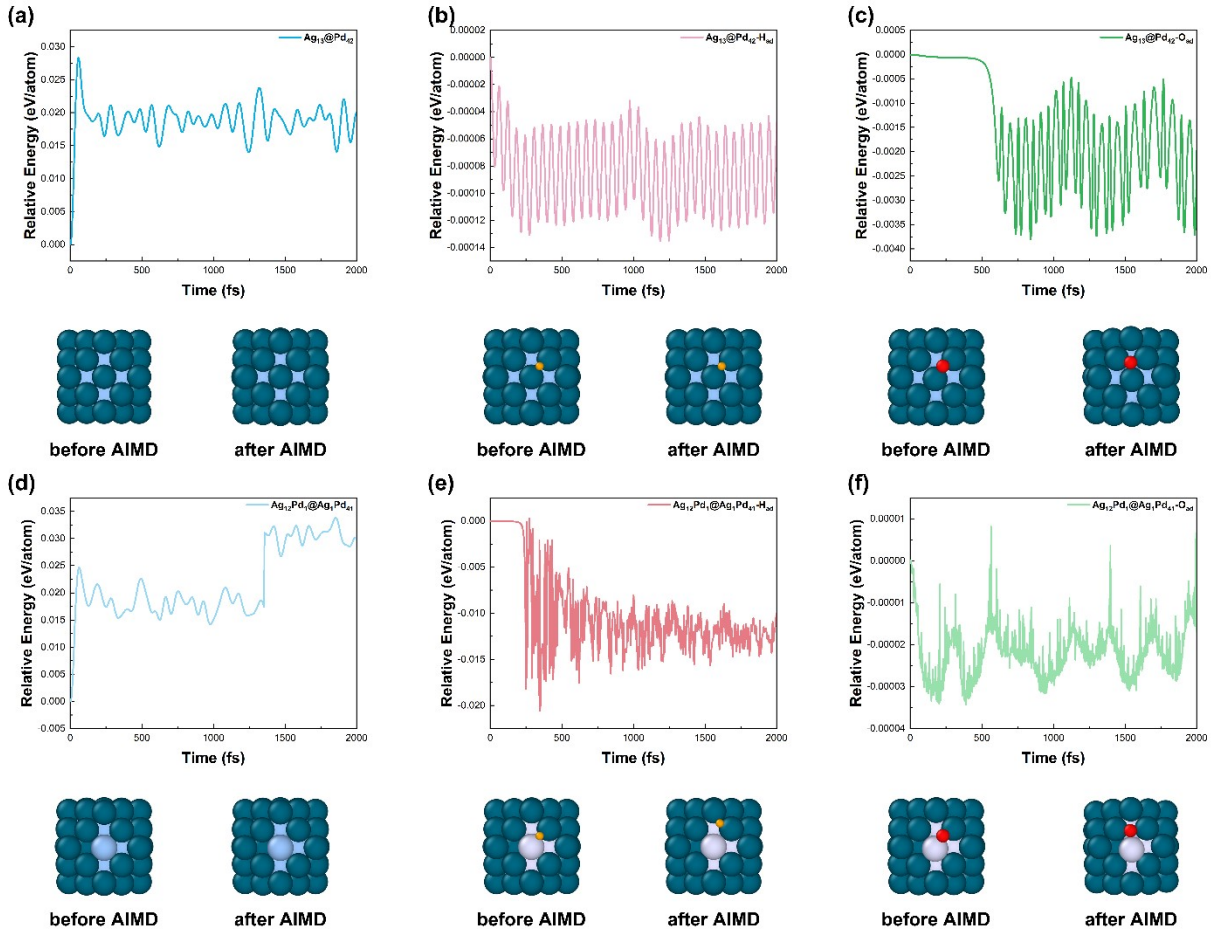

Fig. S7 The relative energy versus the time for AIMD simulations of the (a, b, c) $Ag_{13}@Pd_{42}$ nanoalloy in Oh shape under vacuum, H and O environment, (d, e, f) $Ag_{12}Pd_1@Ag_1Pd_{42}$ nanoalloy in Oh shape under vacuum, H and O environment. The bottom is a schematic of the atomic structure of the core-shell Ag@Pd nanoalloy before and after the AIMD simulation.

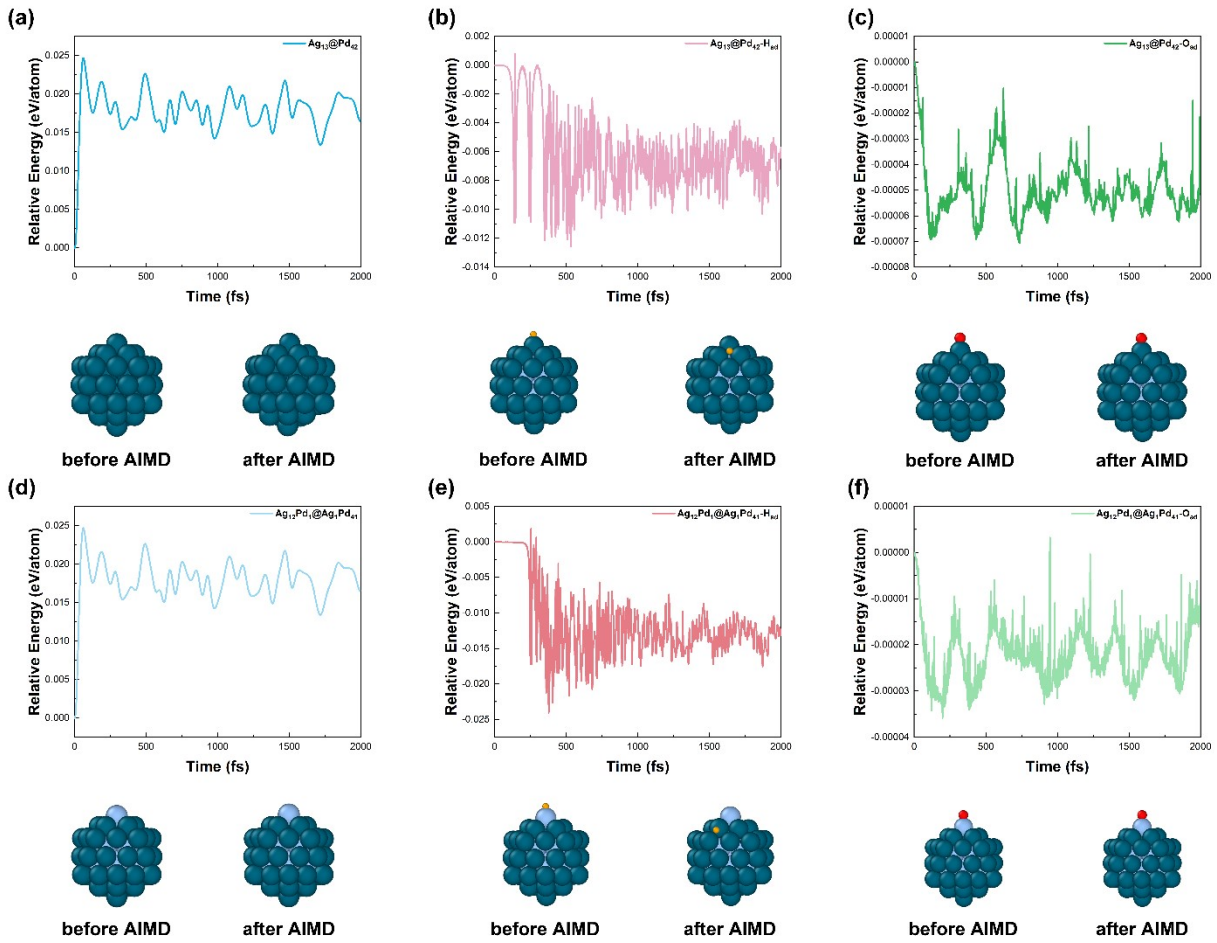

Fig. S8 The relative energy versus the time for AIMD simulations of the (a, b, c) $Ag_{13}@Pd_{42}$ nanoalloy in Ih shape under vacuum, H and O environment, (d, e, f) $Ag_{12}Pd_1@Ag_1Pd_{42}$ nanoalloy in Ih shape under vacuum, H and O environment. The bottom is a schematic of the atomic structure of the core-shell Ag@Pd nanoalloy before and after the AIMD simulation.

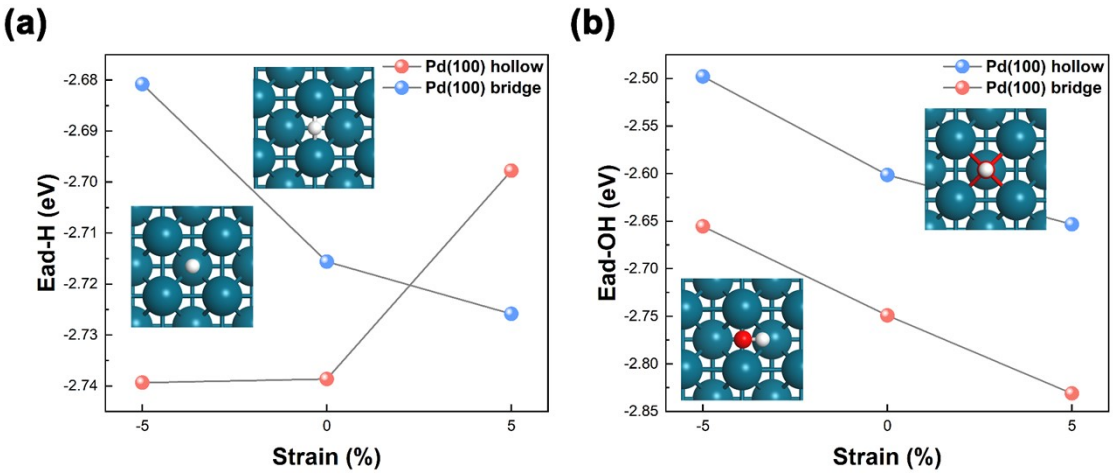

Fig. S9 The H (a) and OH (b) adsorption energy of Pd(100) surface with various strain. The inset displays the atomic structure in the top view of the hollow and bridge adsorption sites.

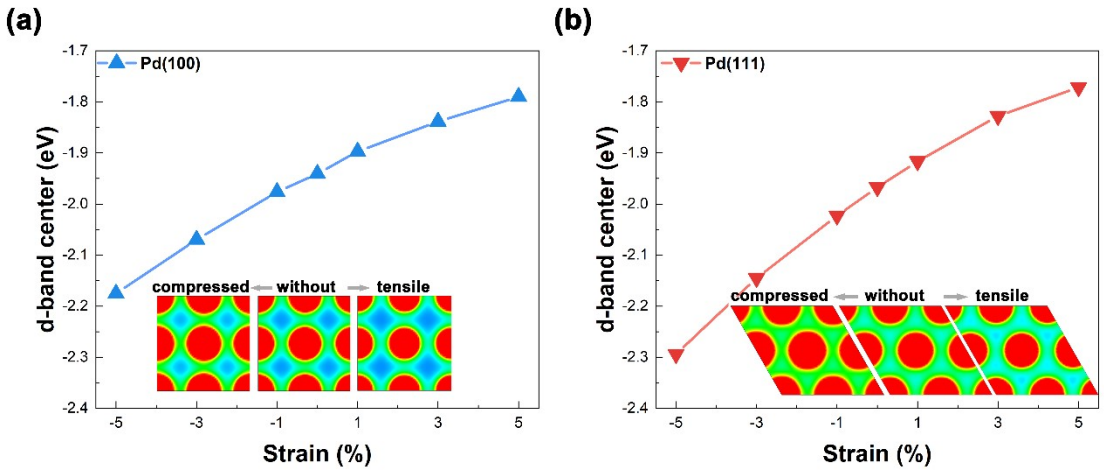

Fig. S10 The d-band center of the (a) Pd(100) and (b) Pd(111) surface as a function of strain. The insets: top views of the electron density plots of the −5% compressed (left), equilibrium (middle), and 5% tensile (right) surfaces.

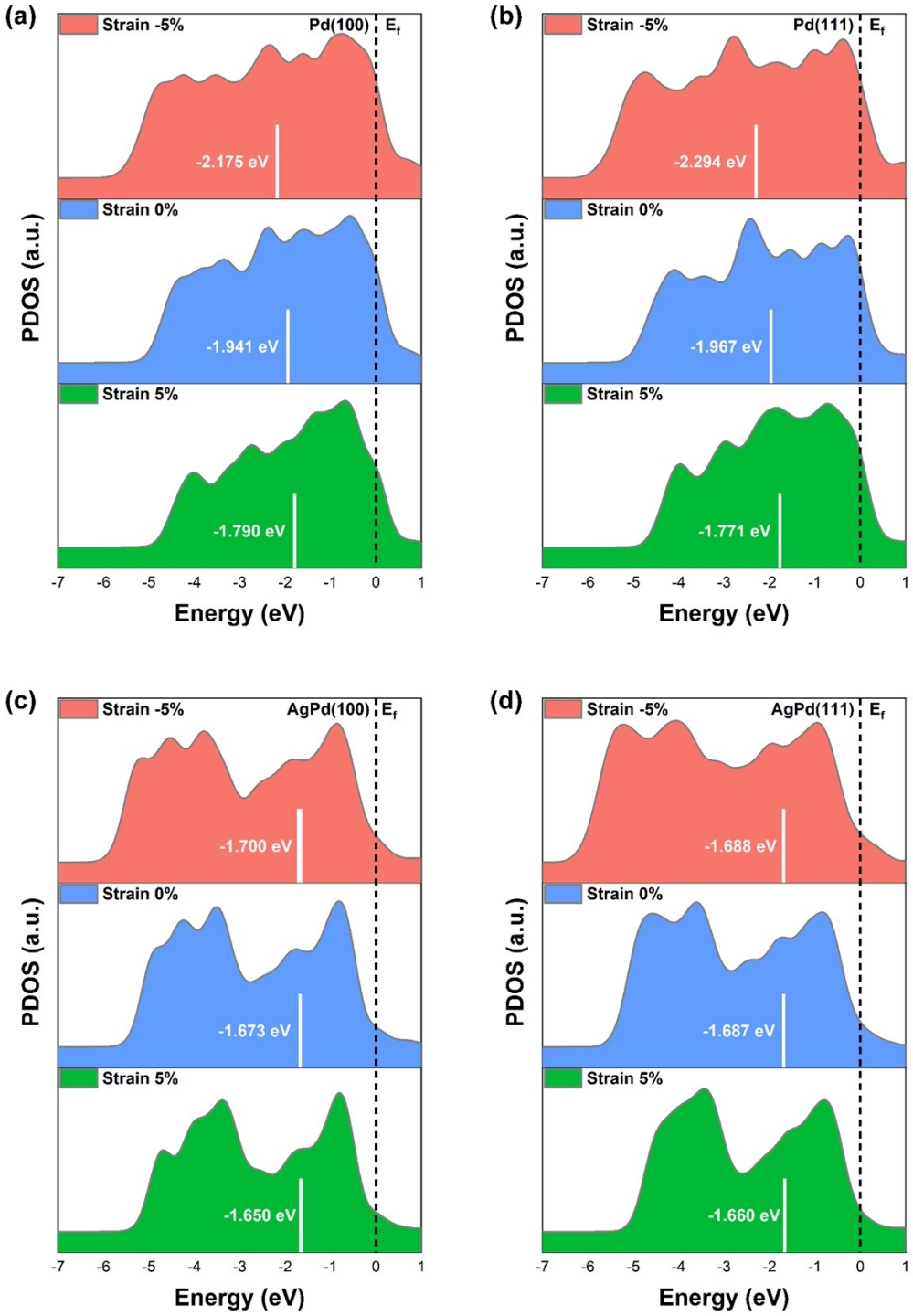

Fig. S11 The partial density of states (PDOS) and d-band center of (a) Pd(100), (b) Pd(111), (c) AgPd(100), and (d) AgPd (111) surfaces with various strain.

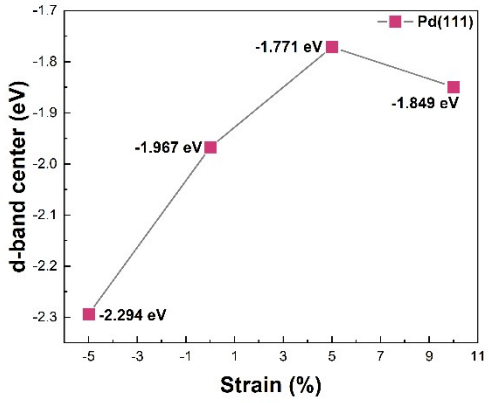

Fig. S12 The d-band center of Pd(111) surfaces with strain range from -5% to 10%.

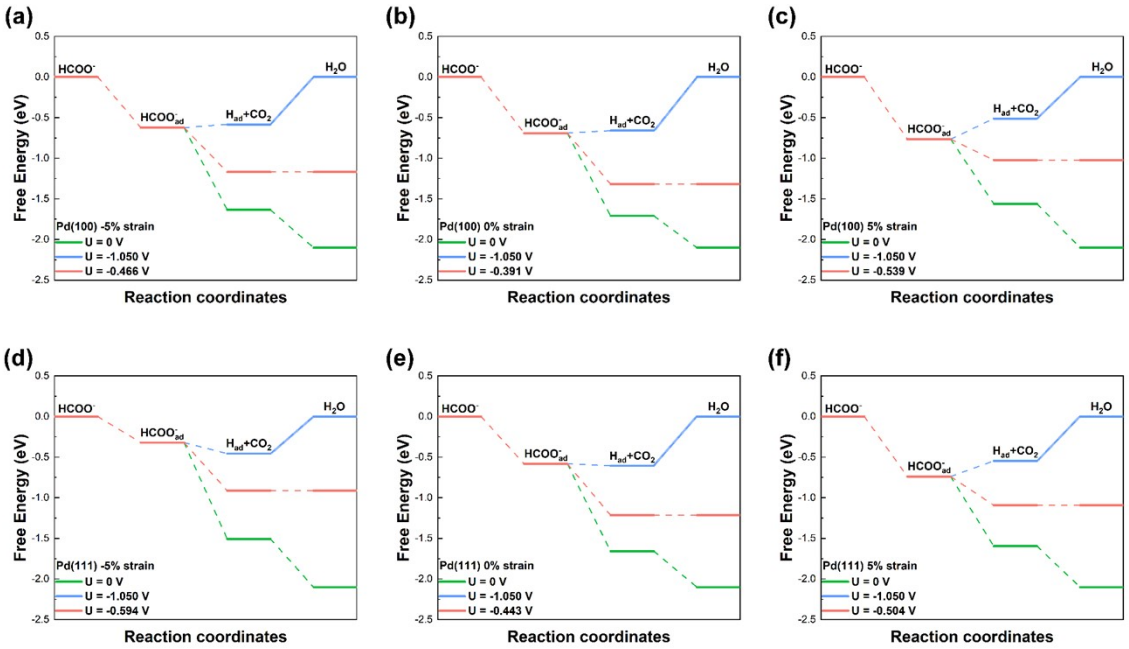

Fig. S13 The free energy diagram for the FOR under various conditions, including zero potential (U = 0 V), equilibrium potential (U_0 = -1.05 V), and overpotential at pH 14 and T=298.15 K on Pd(100) and Pd(111) surfaces with various strain.

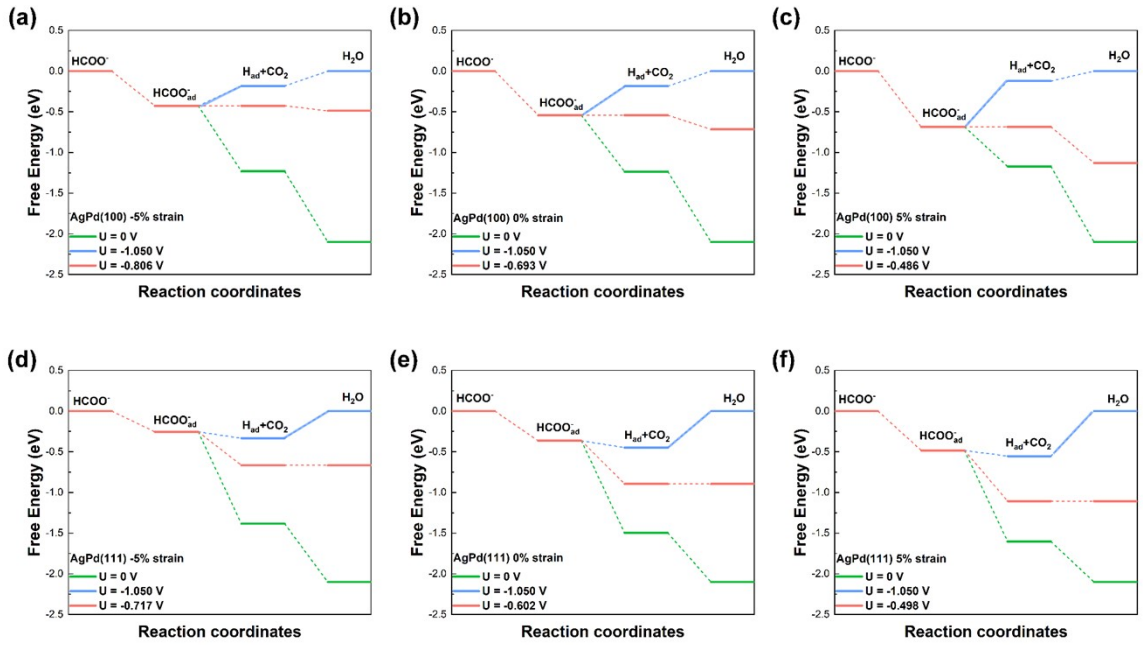

Fig. S14 The free energy diagram for the FOR under various conditions, including zero potential (U = 0 V), equilibrium potential (U_0 = -1.05 V), and overpotential at pH 14 and T=298.15 K on AgPd(100) and AgPd(111) surfaces with various strain.

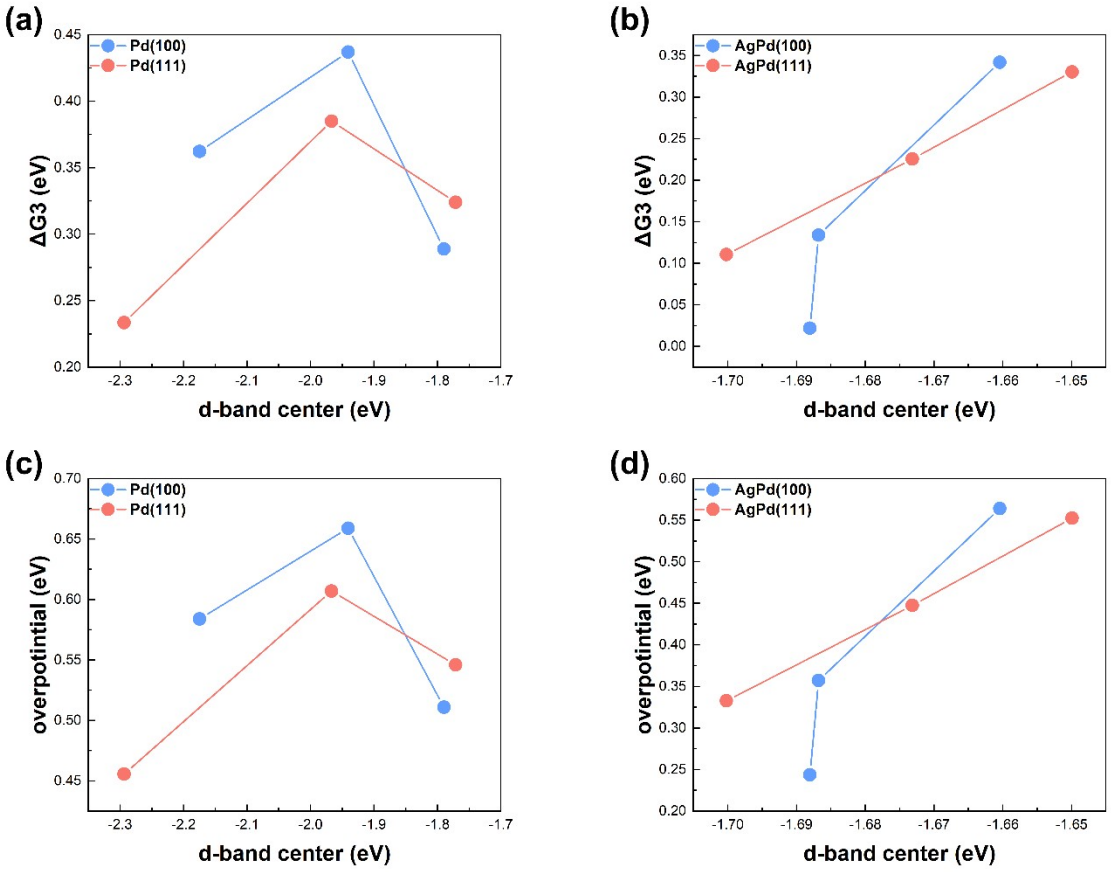

Fig. S15 The ΔG3 of the FDH of (a) Pd nanoalloys and (b) AgPd nanoalloys versus the center of the d-band. The FOR overpotential of (c) Pd nanoalloys and (d) AgPd nanoalloys versus d-band center.

Reference

1 J. K. Nørskov, J. Rossmeisl, A. Logadottir, L. Lindqvist, J. R. Kitchin, T. Bligaard and H. Jónsson, *J. Phys. Chem. B*, 2004, **108**, 17886–17892.

2 N. Zhang, F. Chen, X. Wu, Q. Wang, A. Qaseem and Z. Xia, *J. Mater. Chem. A*, 2017, **5**, 7043–7054.

3 I. C. Man, H.-Y. Su, F. Calle-Vallejo, H. A. Hansen, J. I. Martínez, N. G. Inoglu, J. Kitchin, T. F. Jaramillo, J. K. Nørskov and J. Rossmeisl, *ChemCatChem*, 2011, **3**, 1159–1165.

4 S. M. Foiles, M. I. Baskes and M. S. Daw, *Phys. Rev. B*, 1988, **37**, 10378–10378.

5 F. Cleri and V. Rosato, *Phys. Rev. B*, 1993, **48**, 22–33.

6 F. Baletto, C. Mottet and R. Ferrando, *Phys. Rev. B*, 2002, **66**, 155420.